Inorganic Chemistry
Article

Inorg. Chem. **2010**, *49*, 6153–6159 **6153**
DOI: 10.1021/ic100766d

Synthesis, Characterization, and Computational Study of $MoSF_4$

Jared Nieboer,[†] Johnathan P. Mack,[†] Hélène P. A. Mercier,[‡] and Michael Gerken*[,†]

[†]*Department of Chemistry and Biochemistry, The University of Lethbridge, Lethbridge, Alberta T1K 3M4, Canada, and* [‡]*Department of Chemistry, McMaster University, Hamilton, Ontario L8S 4M1, Canada*

Received April 21, 2010

Molybdenum sulfide tetrafluoride was synthesized from MoF_6 and $S(Si(CH_3)_3)_2$ in $CFCl_3$ at low temperature and was fully characterized by Raman, infrared, and ^{19}F NMR spectroscopy and by X-ray crystallography. The crystal structure revealed that $MoSF_4$ forms infinite fluorine-bridged chains. Quantum-chemical calculations using B3LYP and PBE1PBE methods were used to calculate the gas-phase geometry and vibrational frequencies of monomeric $MoSF_4$ and $(MoSF_4)_3F^-$. The vibrational frequencies of $(MoSF_4)_3F^-$ have been used in the assignment of the vibrational spectra of solid $MoSF_4$. Natural bond order analyses were carried out for monomeric $MoSF_4$ and, for comparison, for WSF_4.

Introduction

Studies of the chemistry of transition-metal sulfide fluorides have mainly focused on the synthesis of WSF_4 while the lighter congener, $MoSF_4$, has received little attention. The only report found in the literature of the synthesis of solid $MoSF_4$ utilizes a high-temperature reaction of MoF_6 and Sb_2S_3.[1] The poor characterization by infrared spectroscopy and mass spectrometry, which showed significant amounts of hydrolysis products, rendered the report inconclusive. Molybdenum sulfide tetrafluoride has also been observed in the gas-phase by mass spectrometry above $MoSF_3$.[2]

The goal of the current study was to find a synthetic route to bulk quantities of $MoSF_4$ and to structurally characterize $MoSF_4$, as the first unambiguously identified molybdenum sulfide fluoride.

Results and Discussion

Synthesis of $MoSF_4$. Yellow-brown $MoSF_4$ was synthesized by the reaction of MoF_6 and $S(Si(CH_3)_3)_2$ in $CFCl_3$ solvent (eq 1). The reaction started at −120 °C before the solvent had melted and had to be quenched with liquid nitrogen intermittently.

$$MoF_6 + S(Si(CH_3)_3)_2 \xrightarrow{CFCl_3} MoSF_4 + FSi(CH_3)_3 \quad (1)$$

Molybdenum sulfide tetrafluoride changed its color to darker shades of brown upon storage at room temperature.

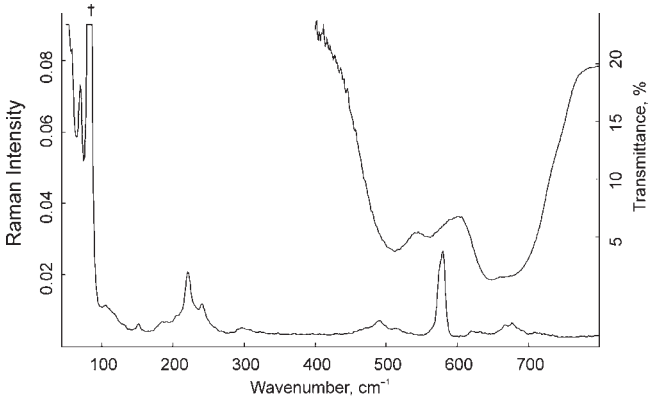

Figure 1. Vibrational spectra of $MoSF_4$: Raman spectrum (lower trace) recorded at room temperature using 1064-nm excitation and the infrared spectrum (upper trace) recorded at room temperature in a KBr pellet. Dagger (†) denotes an instrumental artifact.

The same behavior has been observed for WSF_4.[3] The moderate solubility of $MoSF_4$ in HF and CH_3CN solvents suggests the formation of HF solvates and the formation of the $MoSF_4 \cdot CH_3CN$ adduct, respectively. In CH_3CN solvent, $MoSF_4$ gave rise to a ^{19}F chemical shift at 155.0 ppm, which is attributed to the $MoSF_4 \cdot CH_3CN$ adduct, by analogy with the adduct formation for WSF_4 in CH_3CN ($\delta(^{19}F) = 85.4$ ppm).[3] No coupling to ^{95}Mo was observed as a consequence of rapid quadrupolar relaxation of the ^{95}Mo nuclear spin in the large-efg environment of $MoSF_4 \cdot CH_3CN$. In contrast to WSF_4, no ^{19}F chemical shift was observed for $MoSF_4$ in a HF solvent, which is likely a result of rapid chemical exchange.

Vibrational Spectroscopy. The Raman and infrared spectra of solid $MoSF_4$ are shown in Figure 1. The observed vibrational frequencies of $MoSF_4$ and their assignments are summarized in Table 1 together with the

*To whom correspondence should be addressed. Phone: +1-403-329-2173. Fax: +1-403-329-2057. E-mail: michael.gerken@uleth.ca.

(1) Holloway, J. H.; Puddick, D. C. *Inorg. Nucl. Chem. Lett.* **1979**, *15*, 85–87.
(2) Malkerova, I. P.; Alikhanyan, A. S.; Gorgoraki, V. I. *Russ. J. Inorg. Chem.* **1980**, *25*, 1742–1746. Malkerova, I. P.; Alikhanyan, A. S.; Gorgoraki, V. I. *Zh. Neorg. Khim.* **1980**, *25*, 3181–3187.
(3) Nieboer, J.; Hillary, W.; Yu, X.; Mercier, H. P. A.; Gerken, M. *Inorg. Chem.* **2009**, *48*, 11251–11258.

Published on Web 06/08/2010

Table 1. Experimental Vibrational Frequencies and Assignments for Solid, Polymeric $MoSF_4$ and Calculated Vibrational Frequencies and Assignments for $(MoSF_4)_3F^-$ and Monomeric $MoSF_4$

Polymeric $MoSF_4$			$(MoSF_4)_3F^-$			Monomeric $MoSF_4$		
freq (exptl)[a,b]			freq (calcd)[a,c]			freq (calcd)[a,c]		
Raman[d,e]	infrared[f]	infrared[g]	B3LYP	PBE1PBE	assgnts (C_1)[h]	B3LYP	PBE1PBE	assgnts (C_{4v})[h]
710(3)			685(7)[65]	706(5)[58]	$\nu(Mo_bF_{t1} + Mo_bF_{t2})$			
		690 s	699(2)[489]	717(2)[507]	$\nu(Mo_bF_{t1} - Mo_bF_{t2})$			
678(17)			676(4)[372]	695(3)[395]	νMo_bF_{t3}	704(2)[237]	723(2)[241]	$\nu_7(E)$, $\nu_{as}(MoF_4)$
668(14)	677sh	670 s	665(26)[168]	685(24)[179]	$\nu(Mo_bF_{t1} + Mo_bF_{t3})$	701(11)[126]	722(9)[142]	$\nu_1(A_1)$, $\nu_s(MoF_4)$
	649 vs	633 s	639(3)[52]	657(2)[42]	$\nu(Mo_bF_{t1} + Mo_bF_{t2} + Mo_bF_{b2} - Mo_bF_{t3})$	596(5)[0]	612(4)[0]	$\nu_4(B_1)$, $\nu_{as}(MoF_4)$
621(7)			620(6)[141]	639(5)[135]	$\nu(Mo_1F_{b1} - Mo_bF_{b1})$			
581(100)	580 sh		577(51)[82]	599(45)[91]	$\nu(Mo_bS_t + Mo_bF_{b1})$	605(33)[31]	627(32)[34]	$\nu_2(A_1)$, ν(MoS)
577sh			586(48)[70]	606(49)[86]	$\nu(Mo_bF_{b2} + Mo_bF_{t3})$			
	563 s	564						
514(7)	513 vs		518(24)[32]	536(25)[15]	$\nu(Mo_bF_{b1} + Mo_bF_{b2}) - \nu(Mo_1F_{b1} - Mo_2F_{b2})$			
492(17)		500	511(51)[214]	522(36)[231]	$\nu(Mo_bF_{b2} - Mo_2F_{b2})$			
472sh								
		458	435(9)[395]	445(9)[401]	$\nu(Mo_bF_{b1} - Mo_1F_{b1})$			
			313(2)[3]	324(2)[3]	$\nu(Mo_bF_{b1} + Mo_1F_{b1})$			
			298(<1)[<1]	305(<1)[<1]	$\delta(F_{t2}Mo_bF_{t3}) + \delta(F_{t1}Mo_bF_{b2})$	331(2)[0]	338(2)[0]	$\nu_6(B_2)$, $\delta_{scissoring}(MoF_4)$
298(7)			277(2)[32]	282(2)[29]	$\delta(Mo_bF_{b1}F_{t1}F_{t2}F_{t3})_{umb}$	257(2)[3]	260(2)[3]	$\nu_3(A_1)$, $\delta_{umbrella}(MoF_4)$
			257(2)[20]	263(2)[18]	$\delta(Mo_bF_{b1}F_{t1}F_{t2}F_{t3})_{umb}$			
242(35)			247(3)[4]	251(2)[5]	$\rho_w(F_{t1}Mo_bF_{t2})$	242(<1)[16]	245(<1)[17]	$\nu_8(E)$, $\delta_{in\text{-}plane}(MoF_4)$
			245(1)[10]	248(1)[10]	$\delta(S_tMo_bF_{t2}) + \rho_w(F_{t3}Mo_bF_{b2}) - \delta(S_tMo_bF_{t1})$			
222(72)			230(2)[7]	233(2)[6]	$(MoSF_4)_3F^-$ def.	208(5)[<1]	211(4)[<0.1]	$\nu_9(E)$, δ(SMoF)
			224(3)[4]	227(2)[3]				
207(19)			219(2)[3]	222(2)[3]				
192(11)			211(5)[27]	215(5)[17]				
186(11)			204(1)[23]	207(1)[24]				
			191(<1)[41]	194(<1)[29]				
			187(1)[42]	190(1)[68]	$\rho_w(F_{t1}Mo_bF_{t2}) - \rho_w(F_{t3}Mo_bF_{b2})$			
153(8)								
						115(<1)[0]	116(<1)[0]	$\nu_5(B_1)$, $\delta_{out\text{-}of\text{-}plane}(MoF_4)$
106(8)								
71(83)					lattice modes			
59(5)								

[a] Frequencies are given in cm^{-1}. [b] Abbreviation denotes shoulder (sh), very strong (vs), strong (s), medium (m), weak (w), very weak (vw). [c] Stuttgart f (Mo) and aug-cc-pVTZ (F,S) basis sets. Values in parentheses denote Raman intensities ($Å^4\,u^{-1}$). Values in square brackets denote infrared intensities ($km\,mol^{-1}$). [d] Values in parentheses denote relative Raman intensities. [e] The Raman spectrum of solid $MoSF_4$ was recorded in a sealed melting point capillary at room temperature using 1064-nm excitation. An instrumental artifact was observed at 84 cm^{-1}. [f] The infrared spectrum of $MoSF_4$ was recorded on a KBr pellet at room temperature. [g] Values from ref 1. [h] The atom numbering scheme refers to that used in Figure 2. The abbreviations denote symmetric (s), asymmetric (as), stretch (ν), bend (δ), and wagging (ρ_w). The abbreviation, def., denotes a deformation mode. The in-plane and out-of-plane mode descriptions are relative to the MoF_4 plane.

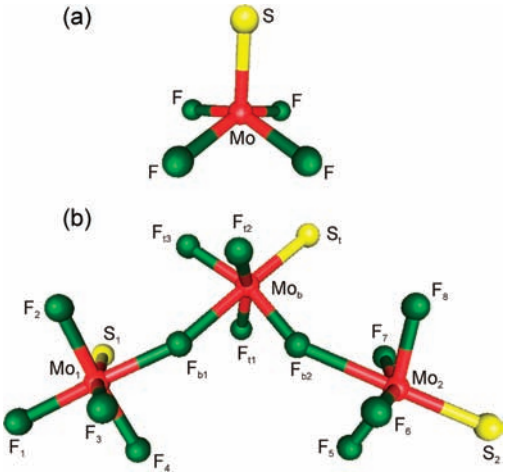

Figure 2. Calculated gas-phase geometries for (a) $MoSF_4$ and (b) $(MoSF_4)_3F^-$.

calculated frequencies and their assignments for monomeric $MoSF_4$ and $(MoSF_4)_3F^-$.

The vibrations of monomeric $MoSF_4$ (Figure 2a) span the reducible representation $\Gamma = 3A_1 + 2B_1 + B_2 + 3E$ under C_{4v} point symmetry. All vibrational modes are Raman active, while the A_1 and E modes are infrared active. Interestingly, the calculated frequency for the asymmetric MoF_4 stretching mode, $\nu_4(B_1)$, is very close to that for the Mo−S stretching mode. The formation of a fluorine-bridged chain of $MoSF_4$ moieties in the solid state (see Crystal Structure of $MoSF_4$) results in lowering of the symmetry from C_{4v} to C_1 and, as a consequence, in the splitting of degenerate modes when compared with those of the monomer. In addition, extensive vibrational mixing between fluorine-bridged $MoSF_4$ moieties is expected and results in its complex Raman and infrared spectra. The overlapping ranges of Mo−S and Mo−F stretching frequencies further complicate the assignments of the experimental vibrational spectra of $(MoSF_4)_\infty$. To reproduce and assign the experimental vibrational frequencies of solid $(MoSF_4)_\infty$, the vibrational frequencies of the unknown, geometry-optimized oligomeric $(MoSF_4)_3F^-$ anion (Figure 2b) were calculated (Table 1 and Supporting Information, Table S2). Since the negative charge is mainly dispersed onto the lighter atoms of the terminal $MoSF_5$ moieties, the vibrational frequencies of the central $MoSF_5$ moiety can be compared to the experimental values of $(MoSF_4)_\infty$. This approach has been proven to be useful for the assignment of the Raman spectrum of $(OsO_3F_2)_\infty$.[4]

The Raman spectrum of $(MoSF_4)_\infty$ is dominated by an intense band at 581 cm^{-1} which can be attributed to the Mo−S stretching modes. This frequency is in good agreement with the calculated value of 605 cm^{-1} (B3LYP) for monomeric $MoSF_4$, and 577 cm^{-1} (B3LYP) for the central Mo environment in $(MoSF_4)_3F^-$. The lower calculated frequency for the $(MoSF_4)_3F^-$ anion compared to that for monomeric $MoSF_4$ is expected because the negative ionic charge results in more polar bonding throughout the oligomeric anion. The observation of a shoulder at 577 cm^{-1} in the Raman spectrum of $(MoSF_4)_\infty$ could be a consequence of vibrational coupling between the adjacent, fluorine-bridged $MoSF_4$ unit, which is supported by the distinctly different calculated Mo−S stretching frequencies for the terminal Mo environments in $(MoSF_4)_3F^-$ compared to that of the central Mo environment, or contributions from Mo−F stretching modes. The experimental bands between 621 and 710 cm^{-1} can be assigned to terminal Mo−F stretching modes, based on the calculated frequencies for $\nu_1(A_1)$ and $\nu_7(E)$ for monomeric $MoSF_4$ and those for the central unit in $(MoSF_4)_3F^-$ between 620 and 685 cm^{-1} (B3LYP). The mode descriptions for $(MoSF_4)_3F^-$ suggest some contribution of Mo−F_{bridge} and Mo---F_{bridge} stretching to the experimental band at 621 cm^{-1} in the Raman spectrum of $(MoSF_4)_\infty$. The observed Raman bands at 472, 492, and 514 cm^{-1} do not have equivalent calculated frequencies for monomeric $MoSF_4$ and can be attributed to Mo---F_{bridge} and Mo−F_{bridge} stretching modes, corroborating the fluorine-bridged chain structure found by X-ray crystallography. The assignment of these stretches is confirmed by the calculated Mo---F_{bridge} and Mo−F_{bridge} stretching modes for $(MoSF_4)_3F^-$ between 313 and 518 cm^{-1} (B3LYP). The assignment of the bands observed below 298 cm^{-1} is complicated by the fact that considerable mixing occurs among the deformation modes. The intense band at 222 cm^{-1} is assigned to a bending mode, derived from the δ(SMoF) mode for monomeric $MoSF_4$, which is predicted to occur at 208 cm^{-1} (B3LYP) as a strong band in the Raman spectrum. Moreover, the calculated frequencies at 224 and 230 cm^{-1} (B3LYP) for $(MoSF_4)_3F^-$ also have some contribution from δ(SMoF). The band observed at 298 cm^{-1} is assigned to an umbrella mode, by comparison with the $\nu_3(A_1)$ mode predicted at 257 cm^{-1} (B3LYP) in monomeric $MoSF_4$, and by comparison with the modes predicted at 257 and 277 cm^{-1} (B3LYP) in $(MoSF_4)_3F^-$.

Compared to $MoOF_4$, which also adopts a polymeric, fluorine-bridged structure in the solid state, the Mo−F stretching bands in $(MoSF_4)_\infty$ are shifted to lower frequencies. This shift reflects the lower electronegativity of sulfur compared to that of oxygen which results in less polar Mo−F bonds in $(MoOF_4)_\infty$. The Raman spectrum of solid $(MoOF_4)_\infty$ also displays bands between 506 and 571 cm^{-1} attributable to Mo---F_{bridge} stretching modes, which are shifted to higher frequencies relative to those of the sulfide analogue.[5]

Table 2. Summary of Crystal Data and Refinement Results for $MoSF_4$

chemical formula	F_4MoS
space group	$Pca2_1$ (No.29)
a (Å)	10.9921(8)
b (Å)	8.2957(6)
c (Å)	27.774(2)
α (deg)	90
β (deg)	90
γ (deg)	90
V (Å^3)	2532.6(3)
Z (molecules/unit cell)	24
mol wt	204.00
calculated density (g cm^{-3})	3.210
T (°C)	−120
μ (mm^{-1})	3.542
R_1[a]	0.0224
wR_2[b]	0.0408

[a] R_1 is defined as $\sum||F_o| - |F_c||/\sum|F_o|$ for $I > 2\sigma(I)$. [b] wR_2 is defined as $[\sum w(F_o^2 - F_c^2)^2/\sum w(F_o^2)^2]^{1/2}$ for $I > 2\sigma(I)$.

(4) Hughes, M. J.; Mercier, H. P. A.; Schrobilgen, G. J. *Inorg. Chem.* **2009**, *48*, 4478–4490.

(5) Fawcett, J.; Holloway, J. H.; Russell, D. R. *J. Chem. Soc., Dalton Trans.* **1981**, 1212–1218.

Table 3. Experimental Geometric Parameters for $MoSF_4$[a]

Bond Lengths (Å)[b]											
Mo1−S1	2.0564(12)	Mo2−S2	2.0616(13)	Mo3−S3	2.0660(13)	Mo4−S4	2.0650(13)	Mo5−S5	2.0646(12)	Mo6−S6	2.0587(11)
Mo1−F11	1.936(3)	Mo2−F21	1.926(3)	Mo3−F31	1.948(2)	Mo4−41	1.943(2)	Mo5−F51	1.930(3)	Mo6−F61	1.930(3)
Mo1−F12	1.824(3)	Mo2−F22	1.822(2)	Mo3−F32	1.845(3)	Mo4−F42	1.841(2)	Mo5−F52	1.835(2)	Mo6−F62	1.840(3)
Mo1−F13	1.809(3)	Mo2−*F*23	1.844(3)	Mo3−F33	1.826(3)	Mo4−F43	1.827(3)	Mo5−F53	1.836(3)	Mo6−F63	1.831(3)
Mo1−F14	1.821(3)	Mo2−F24	1.844(3)	Mo3−F34	1.831(3)	Mo4−F44	1.830(3)	Mo5−F54	1.839(2)	Mo6−F64	1.847(3)
Mo1---F21	2.291(3)	Mo2---F31	2.254(3)	Mo3---F11^{i}	2.256(3)	Mo4---F51	2.296(2)	Mo5---F61	2.257(3)	Mo6---F41^{ii}	2.290(2)
Bond Angles (deg)[b]											
F11−Mo1−S1	98.30(9)	F21−Mo2−S2	99.66(10)	F31−Mo3−S3	96.67(9)	F41−Mo4−S4	99.15(8)	F51−Mo5−S5	98.30(8)	F61−Mo6−S6	97.56(9)
F12−Mo1−S1	99.67(11)	F22−Mo2−S2	100.54(9)	F32−Mo3−S3	101.67(9)	F42−Mo4−S4	100.85(10)	F52−Mo5−S5	99.65(9)	F62−Mo6−S6	100.10(9)
F13−Mo1−S1	101.30(11)	*F*23−Mo2−S2	100.12(9)	F33−Mo3−S3	101.63(12)	F43−Mo4−S4	100.71(11)	F53−Mo5−S5	100.54(11)	F63−Mo6−S6	100.64(11)
F14−Mo1−S1	101.66(11)	F24−Mo2−S2	100.20(10)	F34−Mo3−S3	100.11(10)	F44−Mo4−S4	100.36(10)	F54−Mo5−S5	100.75(10)	F64−Mo6−S6	101.56(9)
S1−Mo1---F21	174.95(8)	S2−Mo2---F31	178.46(8)	S3−Mo3---F11^{i}	175.46(10)	S4−Mo4---F51	176.77(7)	S5−Mo5---F61	176.11(9)	S6−Mo6---F41^{ii}	175.60(8)
Mo1−F11---Mo3^{iii}	153.15(16)	Mo2−F21---Mo1	151.60(14)	Mo3−F31---Mo2	154.98(13)	Mo4−F41---Mo6^{iv}	149.07(13)	Mo5−F51---Mo4	158.18(14)	Mo6−F61---Mo5	163.58(17)
F13−Mo1−F14	91.9(2)	F22−Mo2−*F*23	90.87(12)	F33−Mo3−F34	92.48(17)	F43−Mo4−F44	92.88(15)	F52−Mo5−F53	90.67(13)	F63−Mo6−F62	91.40(15)
F13−Mo1−F12	91.7(2)	F22−Mo2−F24	158.76(13)	F33−Mo3−F32	91.08(15)	F43−Mo4−F42	90.77(14)	F52−Mo5−F54	159.05(12)	F63−Mo6−F64	89.58(14)
F14−Mo1−F12	157.20(15)	*F*23−Mo2−F24	89.94(14)	F34−Mo3−F32	156.73(12)	F44−Mo4−F42	157.41(13)	F53−Mo5−F54	90.29(13)	F62−Mo6−F64	157.75(11)
F13−Mo1−F11	160.39(13)	F22−Mo2−F21	86.18(12)	F33−Mo3−F31	161.58(14)	F43−Mo4−F41	160.04(12)	F52−Mo5−F51	87.66(12)	F63−Mo6−F61	161.72(13)
F14−Mo1−F11	83.73(17)	*F*23−Mo2−F21	160.21(12)	F34−Mo3−F31	86.30(13)	F44−Mo4−F41	85.48(13)	F53−Mo5−F51	161.10(12)	F62−Mo6−F61	87.09(14)
F12−Mo1−F11	85.30(18)	F24−Mo2−F21	85.91(14)	F32−Mo3−F31	83.14(11)	F42−Mo4−F41	83.55(12)	F54−Mo5−F51	84.71(12)	F64−Mo6−F61	85.08(14)
F13−Mo1---F21	82.48(12)	F22−Mo2---F31	79.76(10)	F33−Mo3---F11^{i}	82.88(15)	F43−Mo4---F51	82.47(11)	F52−Mo5---F61	78.32(11)	F63−Mo6---F41^{ii}	83.24(12)
F14−Mo1---F21	81.44(13)	*F*23−Mo2---F31	81.37(11)	F34−Mo3---F11^{i}	79.05(12)	F44−Mo4---F51	78.85(12)	F53−Mo5---F61	82.87(13)	F62−Mo6---F41^{ii}	77.62(10)
F12−Mo1---F21	76.75(13)	F24−Mo2---F31	79.38(12)	F32−Mo3---F11^{i}	78.59(11)	F42−Mo4---F51	79.55(11)	F54−Mo5---F61	81.03(11)	F64−Mo6---F41^{ii}	80.42(10)
F11−Mo1---F21	77.98(11)	F21−Mo2---F31	78.84(10)	F31−Mo3---F11^{i}	78.84(12)	F41−Mo4---F51	77.69(10)	F51−Mo5---F61	78.36(11)	F61−Mo6---F41^{ii}	78.64(10)

[a] For atom numbering see Figure 3. [b] Symmetry codes: (i) $x-1/2, -y+1. z$; (ii) $x-1/2, -y+2, z$; (iii) $x+1/2, -y+1, z$; (iv) $x+1/2, -y+2, z$.

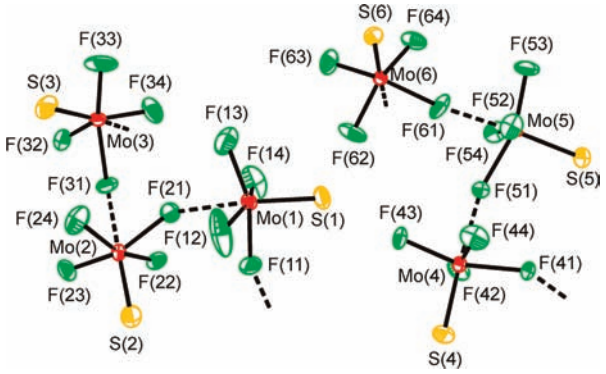

Figure 3. X-ray crystal structure of $MoSF_4$ showing the two crystallographically independent polymer chains; thermal ellipsoids are shown at the 50% probability level.

Crystal Structure of $MoSF_4$. Details of the data collection parameters and other crystallographic information for $MoSF_4$ are given in Table 2 while important bond lengths and angles are listed in Table 3.

Molybdenum sulfide tetrafluoride crystallizes in the orthorhombic space group $Pca2_1$, forming infinite helical chains of *cis*-fluorine-bridged $MoSF_5$ pseudo-octahedra along the *a*-axis (Figure 3 and Supporting Information, Figure S1). Molybdenum sulfide tetrafluoride is isostructural with $ReSF_4$[6] with 24 $MoSF_4$ formula units in the unit cell and two crystallographically independent *cis*-fluorine bridged chains.

In solid $MoSF_4$, the coordination number about Mo is six, because one fluorine of each $MoSF_4$ moiety coordinates to an adjacent Mo center trans to the Mo=S bond. The local environments about the six crystallographically independent Mo centers vary significantly, as indicated by the bond length ranges. Moreover, the Mo−F bridge bonds are asymmetric, with the longer Mo---F_{bridge} bond distances ranging from 2.254(3) to 2.296(2) Å and the shorter Mo−F_{bridge} bond lengths ranging from 1.926(3) to 1.948(2) Å. The latter are elongated compared to the terminal Mo−F bonds which range from 1.809(3) to 1.847(3) Å. The Mo−S bond lengths in $MoSF_4$ range from 2.0569(12) to 2.0658(13) Å and show the smallest variations when compared with the Mo−F bond lengths. The small range in Mo−S bond lengths is likely a consequence of the higher Mo−S bond order in $MoSF_4$ which can be best described as a Mo=S double bond. The thermal ellipsoids of some terminal fluorine atoms are elongated perpendicular to the bonding axis; the ellipsoid elongation of the terminal F(12) and F(13) atoms are particularly significant, indicating residual motion in the crystal structure. The range of Mo−F---Mo bridging angles in $MoSF_4$ is considerable with values from 149.07(13)−163.58(17)°, reflecting the flexibility of this angle. The coordination polyhedron about the molybdenum atoms are distorted octahedra with the apex comprised by the sulfur atom being elongated (Figure 4 and Supporting Information, Figure S2). The terminal fluorines and the bridging fluorine atom of the $MoSF_4$ moiety lie in a plane with mean deviations of 0.0071 to 0.0263 Å with the molybdenum atoms displaced by 0.317 to 0.332 Å above the plane toward the sulfur atoms.

(6) Holloway, J. H.; Kaučič, V.; Russell, D. R. *Chem. Commun.* **1983**, 1079–1081.

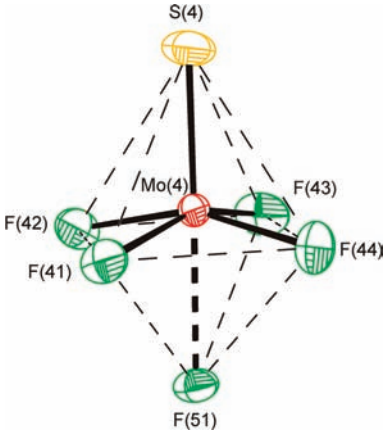

Figure 4. View of the coordination environment about Mo(4) in the X-ray crystal structure of $MoSF_4$; thermal ellipsoids are shown at the 50% probability level.

The oxide analogue, $MoOF_4$, also forms a *cis*-fluorine bridged polymeric chain structure of $MoOF_5$ pseudo-octahedra.[7] The terminal Mo−F bond lengths in $MoSF_4$ are similar to those found for its oxide analogue, $MoOF_4$, (1.82(1)−1.84(1) Å). Surprisingly, the nature of the fluorine-bridging is similar with Mo−F_{bridge} bonds and Mo---F_{bridge} coordinate bonds in $MoSF_4$ and $MoOF_4$ (Mo−F_{bridge}: 1.93(1), 1.96(1) and Mo---F_{bridge}: 2.27(1), 2.31(1) Å). Even the Mo−F---Mo angles, which are expected to be strongly dependent on crystal packing, are comparable, although in a much narrower range in $MoOF_4$ with 151.2(5) and 150.7(5)°. The analogies between $MoSF_4$ and $MoOF_4$ extend to the location of the Mo atoms in the coordination octahedron. In $MoOF_4$, both crystallographically independent Mo atoms are displaced by 0.31 Å above the plane of the fluorine atoms cis to the sulfur; this degree of displacement is surprisingly close to that found for $MoSF_4$.

Computational Results

The electronic structures of monomeric $MoSF_4$ (C_{4v}) and $(MoSF_4)_3F^-$ (C_1) were optimized at the B3LYP and PBE1PBE levels and resulted in stationary points with all frequencies real (Figure 2). The energy-minimized geometries and vibrational frequencies of MoF_6 were also calculated (Supporting Information, Table S1) to serve as a benchmark.

(a) Calculated Geometries. $MoSF_4$. The geometric parameters of monomeric $MoSF_4$ are given in Table 4. The optimized gas-phase geometry of monomeric $MoSF_4$ has a square-pyramidal geometry with C_{4v} point symmetry (Figure 2a). While the values from the PBE1PBE calculations are within the observed ranges of Mo−S and terminal Mo−F bond lengths, the calculated values at the B3LYP level of theory systematically overestimate the bond lengths, as found for MoF_6. The calculated S−Mo−F angles with 105.4 (B3LYP) and 105.6° (PBE1PBE) are larger than those in the fluorine-bridged polymer of solid $MoSF_4$ as a consequence of the absence of a bridging fluorine contact in the gas-phase.

$(MoSF_4)_3F^-$. To model the experimental polymeric $MoSF_4$ structure, the geometry of the unknown oligomeric

(7) Edwards, A. J.; Stevenston, B. R. *J. Chem. Soc., A* **1968**, 2503.

Table 4. Experimental and Calculated Bond Lengths (Å) and Angles (deg) for $MoSF_4$ and $(MoSF_4)_3F^-$

	$MoSF_4$			$(MoSF_4)_3F^-$	
		calcd (monomeric)		calcd (central $MoSF_5$ moiety)	
	exptl (polymeric)	B3LYP	PBE1PBE	B3LYP	PBE1PBE
$Mo-F_{term}$	1.809(3) to 1.847(3)	1.849	1.834	1.849, 1.853	1.833, 1.837
$Mo-F_{bridge}$	1.926(3) to 1.948(2)			1.938	1.925
$Mo---F_{bridge}$	2.254(2) to 2.296(2)			2.191	2.172
Mo−S	2.0564(12) to 2.0660(13)	2.081	2.066	2.101	2.084
F−Mo−S	96.67(10) to 101.67(9)	105.4	105.6	97.5 to 99.8	97.6 to 100.0
$S-Mo---F_{bridge}$	174.95(8) to 178.46(8)			179.0	178.8
cis-$F-Mo-F_{bridge}$	83.14(11) to 87.66(12)			86.2, 86.4	86.0, 86.1
cis-F−Mo−F	89.58(14) to 92.88(15)	86.0	85.9	90.8, 91.0	91.0, 91.1
F−Mo---F	77.62(10) to 83.24(12)			80.1 to 81.6	79.9 to 81.9
Mo−F---Mo	149.07(13) to 163.58(17)			151.5, 158.1	149.1, 154.6

$(MoSF_4)_3F^-$ anion was optimized (Figure 2b). The calculated geometric parameters of the central $MoSF_5$ coordination octahedron in $(MoSF_4)_3F^-$ are listed in Table 4, while the complete list of geometric parameters for $(MoSF_4)_3F^-$ is given in Supporting Information, Table S3. The calculated bond lengths and angles about the central Mo atom of $(MoSF_4)_3F^-$ are in excellent agreement with the experimental values for $(MoSF_4)_\infty$. The calculated $Mo-F_{bridge}$ bond lengths are within the range of the experimental values. The significantly weaker $Mo---F_{bridge}$ bond length is underestimated in the calculations with 2.191 (B3LYP) and 2.172 Å (PBE1PBE) versus 2.254(2) to 2.296(2) Å observed in the crystal structure of $(MoSF_4)_\infty$. The calculated Mo−F---Mo angles in $(MoSF_4)_3F^-$ of 151.5, 158.1° (B3LYP) and 149.1, 154.6° (PBE1PBE) reproduce the experimental angles in $(MoSF_4)_\infty$ extremely well. The overall good agreement of the geometric parameters between the optimized geometry about the central Mo atom in $(MoSF_4)_3F^-$ and the experimental geometry in $MoSF_4$ suggests that the central Mo environment in $(MoSF_4)_3F^-$ is a good model for the polymeric solid-state structure of the neutral compound, $MoSF_4$.

(b) Charges, Valencies, and Bond Orders. Natural bond order analyses were carried out for $MoSF_4$, WSF_4, and $(MoSF_4)_3F^-$. The natural population analysis (NPA) charges, the valencies, and bond orders for $MoSF_4$ and WSF_4 are listed in Table 5. The charges on Mo in $MoSF_4$ are 1.79 (B3LYP) and 1.81 (PBE1PBE), which are lower than those for tungsten in WSF_4, which are 2.10 (B3LYP) and 2.11 (PBE1PBE). The lower charges on Mo are paralleled by lower charges on the fluorine and sulfur in $MoSF_4$ relative to those of WSF_4, reflecting the lower electronegativity of W compared to Mo. The most significant differences between the molybdenum and tungsten sulfide fluorides are the calculated charges on sulfur. While the sulfur atom in WSF_4 is sulfidic with a negative charge of −0.12 (B3LYP) and −0.14 (PBE1PBE), the charges in $MoSF_4$ are close to zero or even positive with 0.03 (B3LYP) and 0.01 (PBE1PBE). The results of the NBO analysis for $(MoSF_4)_3F^-$ are given in Supporting Information, Table S4. When comparing the charges of the lighter atoms, the lighter atoms around Mo_2 and particularly around Mo_1 carry more of the negative charge, than those around Mo_b. The Mo_b---F_{b2} bond was calculated to have a bond order of 0.13 (B3LYP) and 0.15 (PBE1PBE), indicating the weakness of the fluorine bridging found in solid $MoSF_4$.

Table 5. Natural Bond Order (NBO) Valencies, Bond Orders, and Natural Population Analysis (NPA) Charges for $MoSF_4$ and WSF_4

	$MoSF_4$		WSF_4	
	B3LYP	PBE1PBE	B3LYP	PBE1PBE
		NPA Charges		
Mo/W	1.79	1.81	2.10	2.11
S	0.03	0.01	−0.12	−0.14
F	−0.46	−0.45	−0.49	−0.49
		Valencies		
Mo/W	3.50	3.55	3.52	3.56
S	1.26	1.29	1.28	1.29
F	0.59	0.60	0.58	0.60
		Bond Orders		
Mo/W−S	1.20	1.22	1.22	1.24
Mo/W−F	0.58	0.58	0.58	0.58

Conclusions

A synthetic route to $MoSF_4$ has been developed, and the present study presents the first structural characterization of a molybdenum sulfide fluoride. The fluorine-bridged chain structure of $MoSF_4$ parallels the solid-state structure of its oxide analogue, $MoOF_4$. The synthesis of $MoSF_4$ opens up the investigation of the chemistry of molybdenum sulfide fluorides. The NBO analysis of MSF_4 (M = Mo, W) showed that sulfur in the molybdenum species bears no or a slightly positive charge, while the tungsten analogue contains sulfidic, that is, negatively charged, sulfur.

Experimental Section

Materials and Apparatus. All volatile materials were handled (a) on a Pyrex vacuum line equipped with glass/Teflon J. Young valves and (b) a vacuum line constructed of nickel, stainless steel, and FEP. Nonvolatile materials were handled in the dry nitrogen atmosphere of a drybox (Omni Lab, Vacuum Atmospheres). Reaction vessels and NMR sample tubes were fabricated from $^1/_4$-in. o.d. and 4-mm o.d. FEP tubing, respectively, and outfitted with Kel-F valves. All reaction vessels and sample tubes were rigorously dried under dynamic vacuum prior to passivation with 1 atm F_2 gas.

The solvents, CH_3CN (Sigma-Aldrich, HPLC grade) and $CFCl_3$ (Aldrich, 99+%) were dried according to standard literature methods[8] and over CaH_2, respectively. Molybdenum hexafluoride (Elf Atochem) was used without further purification. Hexamethyldisilathiane (Fluka, purum) and Sb_2S_3 (Alfa Aesar,

(8) Winfield, J. M. *J. Fluorine Chem.* **1984**, *25*, 91–98.

99.5%) were purified by vacuum distillation and by drying under dynamic vacuum at 160 °C for about 6 h, respectively.

Preparation of $MoSF_4$. On the glass vacuum line, 5.388 g of $CFCl_3$ was vacuum distilled into a $^3/_4$-in. o.d. FEP reactor with a stainless steel valve containing a small Teflon-coated stir bar. Subsequently, 0.306 g (1.71 mmol) of $S(Si(CH_3)_3)_2$ was vacuum distilled on top of the frozen $CFCl_3$ at −196 °C, and after warming to 20 °C, the resulting solution was stirred for 1 min. A slight excess of MoF_6, 0.410 g (1.95 mmol) was transferred into the reaction vessel at −196 °C. The reaction vessel was allowed to warm toward room temperature very slowly with constant agitation and quenching in liquid N_2 to prevent side-reactions. The reaction mixture changed from colorless to yellow/brown while the solvent was still frozen at temperatures below −120 °C. As the reaction progressed, the reaction mixture changed from colorless to a homogeneous dark purple color which persisted even at room temperature. The dark purple solid settled from the solvent, which was slowly removed into a $^3/_4$-in. o.d. FEP U-tube at −196 °C with other volatile byproduct, yielding 0.300 g (1.47 mmol) of yellow-brown $MoSF_4$ in a 86% yield.

Vibrational Spectroscopy. The Raman spectrum of $MoSF_4$ was recorded on a Bruker RFS 100 FT Raman spectrometer with a quartz beam splitter, a liquid-nitrogen-cooled Ge detector, and a low-temperature accessory. The backscattered (180°) radiation was sampled. The actual usable Stokes range was 50 to 3500 cm^{-1} with a spectral resolution of 2 cm^{-1}. The 1064-nm line of an Nd:YAG laser was used for excitation of the sample. A Raman correction was applied for the Raman spectrum using the white light spectrum of a tungsten lamp. The room-temperature spectrum of $MoSF_4$ was recorded on a powdered sample in a melting point capillary using a laser power of 150 mW. The FT-infrared spectra of $MoSF_4$ were recorded on a Nicolet Avatar 360 FTIR spectrometer at ambient temperature. A KBr sandwich was formed in a Wilks minipress inside the drybox by sandwiching the sample between two layers of KBr disks. The spectra were acquired in 64 scans at a resolution of 2 cm^{-1}.

Nuclear Magnetic Resonance Spectroscopy. All NMR spectra were recorded unlocked on a 300 MHz Bruker Avance II NMR spectrometer equipped with a 5 mm broad band probe. Fluorine-19 (282.404 MHz) NMR spectra were referenced externally to neat $CFCl_3$ at 25 °C. The ^{19}F NMR spectra were typically acquired in 128 K memory with spectral settings of 57 kHz, yielding an acquisition time of 0.38 s and a data point resolution of 1.3 Hz/data point. The number of transients accumulated was 5000 using a pulse width of 10.3 μs.

X-ray Crystal Structure Determination of $MoSF_4$. (a) Crystal Growth and Crystal Mounting. Crystals of $MoSF_4$ were grown in anhydrous HF solvent at a temperature between −53 to −59 °C. A crystal of $MoSF_4$ having the dimensions 0.10 × 0.06 × 0.05 mm^3 was selected at −80 °C for low-temperature X-ray structure determination under a flow of cold nitrogen and mounted as previously described.[9]

(b) Collection and Reduction of X-ray Data. The crystal was centered on a Bruker SMART APEX II diffractometer, equipped with an APEX II 4K CCD area detector and a triple-axis goniometer, controlled by the APEX2 Graphical User Interface (GUI) software,[10] and a sealed source emitting graphite-monochromated Mo−Kα radiation (λ = 0.71073 Å). Diffraction data collection at −120 °C consisted of four ω scans at various φ settings of 366 frames each at a fixed χ = 54.74° with a width of 0.5°. The data collection was carried out in a 512 × 512 pixel mode using 2 × 2 pixel binning. Processing of the raw data was completed by using the APEX2 software,[10] which applied Lorentz and polarization corrections to three-dimensionally integrated diffraction spots. The program SADABS[11] was used for the scaling of diffraction data, the application of a decay correction, and an empirical absorption correction on the basis of the intensity ratios of redundant reflections.

(c) Solution and Refinement of the Structure. The XPREP program was used to confirm the unit cell dimensions and the crystal lattice. The solutions were obtained by direct methods which located the positions of the atoms defining six bridged $MoSF_4$ moieties. The final refinement was obtained by introducing anisotropic thermal parameters and the recommended weightings for all of the atoms. The maximum electron densities in the final difference Fourier map were located near the heavy atoms. All calculations were performed using the SHELXTL-plus package for the structure determination and solution refinement and for the molecular graphics.[12] The choice of the correct space group was confirmed by use of PLATON.[13]

Computational Results. The optimized geometries and frequencies of MoF_6 and $MoSF_4$ were calculated at the density functional theory (DFT) level by use of PBE1PBE and B3LYP[14] methods. The Stuttgart basis set augmented by one f-type polarization function (α_f Mo 1.043)[15] for molybdenum and aug-cc-pVTZ basis sets for sulfur and fluorine was used.

Pseudopotentials were used for molybdenum. Quantum-chemical calculations were carried out using the program Gaussian 03.[14] The levels and basis sets were benchmarked by calculating MoF_6 and comparing with the experimental geometries[16] and vibrational frequencies.[17] The geometries were fully optimized using analytical gradient methods. After optimization at one level of theory, the geometries were calculated at the other level of theory to ensure an equivalent energy-minimized geometry had been achieved. The vibrational frequencies were calculated at the PBE1PBE and B3LYP levels using the appropriate minimized structure, and the vibrational mode descriptions were assigned with the aid of Gaussview.[18]

Acknowledgment. We thank the Natural Sciences and Engineering Research Council of Canada (M.G.), the University of Lethbridge (M.G.), and the Research Corporation (M.G.) for support of this work. J.P.M. thanks the Natural Sciences and Engineering Research Council of Canada and the Fluorine Division of the American Chemical Society for an undergraduate research award and a Moissan fellowship, respectively. The quantum-chemical calculations were carried out using the computational resources of the Shared Hierarchical Academic Research Computing Network (SHARCNET: www.Sharcnet.ca).

Supporting Information Available: View of two crystallographically independent chains of $MoSF_4$ (Figure S1); views of the coordination environments about Mo (Figure S2); benchmark computational study for MoF_6 (Table S1); complete list of calculated frequencies for $(MoSF_4)_3F^-$ (Table S2); calculated bond lengths and bond angles for $(MoSF_4)_3F^-$ (Table S3); NBO analysis for $(MoSF_4)_3F^-$ (Table S4); full version of ref 14; X-ray crystallographic file in CIF format for the structure determination of $MoSF_4$. This material is available free of charge via the Internet at http://pubs.acs.org.

(9) Gerken, M.; Dixon, D. A.; Schrobilgen, G. J. *Inorg. Chem.* **2000**, *39*, 4244–425.
(10) *APEX 2*, Version 2.2-0; Bruker AXS, Inc.: Madison, WI, 2007.
(11) Sheldrick, G. M. *SADABS*, Version, 2007/4; Bruker AXS Inc.: Madison, WI, 2007.
(12) Sheldrick, G. M. *SHELXTL97*; University of Göttingen: Göttingen, Germany, 1997.
(13) Spek, A. L. *J. Appl. Crystallogr.* **2003**, *36*, 7–13.
(14) Frisch, M. J. et al. *Gaussian 03*, revision B.04; Gaussian Inc.: Pittsburgh, PA, 2003.
(15) Ehlers, A. W.; Bohme, M.; Dapprich, S.; Gobbi, A.; Hollwarth, A.; Jonas, V.; Kohler, K. F.; Segmann, R.; Veldkamp, A.; Frenking, G. *Chem. Phys. Lett.* **1993**, *208*, 111–114.
(16) Richardson, A.; Hedberg, K.; Lucier, G. M. *Inorg. Chem.* **2000**, *39*, 2787–2793.
(17) Nagarajan, G.; Adams, T. S. *Z. Phys. Chem.* **1974**, *255*, 869–888.
(18) *GaussView*, release 3.0; Gaussian Inc.: Pittsburgh, PA, 2003.